# Nanoscale optomechanical actuators for controlling mechanotransduction in living cells

Zheng Liu[1,6], Yang Liu[1,6], Yuan Chang[1], Hamid Reza Seyf[2], Asegun Henry[2,3], Alexa L Mattheyses[4], Kevin Yehl[1], Yun Zhang[1], Zhuangqun Huang[5] & Khalid Salaita[1]

**To control receptor tension optically at the cell surface, we developed an approach involving optomechanical actuator nanoparticles that are controlled with near-infrared light. Illumination leads to particle collapse, delivering piconewton forces to specific cell surface receptors with high spatial and temporal resolution. We demonstrate optomechanical actuation by controlling integrin-based focal adhesion formation, cell protrusion and migration, and T cell receptor activation.**



The majority of cells within multicellular organisms experience forces that are highly orchestrated in space and time[1]. Several methods make it possible to investigate the cellular response to spatially confined mechanical inputs[2]. Micropipettes[3] and single-molecule techniques[4,5] are used to physically prod the apical side of cells, but such approaches have low throughput[2]. Magnetic actuation of nanoparticles[6,7] and micropillars[8] can trigger mechanotransduction pathways but require either a sparse density of magnetic elements or sophisticated microfabricated structures that focus an external magnetic field. Therefore, magnetic stimulation of mechanotransduction circuits remains specialized and is not widely used. Manipulating forces with molecular specificity and high spatiotemporal resolution remains a hurdle[2].

Optical approaches for the manipulation of biological systems are rapidly proliferating, as exemplified by caged or photoswitchable molecules and by optogenetic constructs[9–11]. Similarly, methods to harness light for delivering precise physical inputs to biological systems could potentially transform the study of mechanotransduction.

Toward this goal, we develop optomechanical actuator (OMA) nanoparticles to manipulate receptor mechanics with high spatiotemporal resolution using near-infrared (NIR) illumination (**Fig. 1a**). OMA nanoparticles shrink rapidly upon illumination, thereby applying a mechanical load to receptor-ligand complexes decorating the immobilized particle. The NIR optical pulse train controls the amplitude, duration, repetition and loading rate of mechanical input. OMAs are immobilized onto standard glass coverslips, allowing cell imaging and manipulation using a conventional optical microscope equipped with an inexpensive NIR laser. Therefore, cell response to mechanical forces can be characterized with unprecedented spatial and temporal resolution. Because mechanical inputs can be rapidly deployed across arbitrary patterns at the cell surface, we demonstrate optomechanical control of focal adhesion (FA) formation, cell protrusions, cell migration and T cell activation.

OMA nanoparticles are comprised of a gold nanorod (25 × 100 nm) coated with a thermoresponsive polymer (**Fig. 1b** and **Supplementary Fig. 1**). The nanorod functions as a photothermal transducer, converting NIR light to localized heat that drives polymer collapse. OMA particles can be immobilized onto virtually any type of support and can also be functionalized with a variety of small-molecule, peptide and protein ligands specific to a receptor of interest, thereby making the mechanical actuation molecularly selective.

TEM, dynamic light scattering and visible-NIR spectra confirmed the particle structure and thermal response (**Fig. 1b** and **Supplementary Fig. 2**). Immobilized particles collapsed in both the lateral (~120 nm) and vertical (~70 nm) directions, indicating that forces point inward toward the particle center (**Fig. 1c**,**d**). Structured illumination microscopy (SIM) also showed a ~100-nm decrease in diameter following illumination (**Supplementary Fig. 3** and **Supplementary Table 1**). In principle, the magnitude of particle collapse can be tuned by changing the particle size and the illumination profile.

Key to the optomechanical actuation strategy is that particle heating is transient and confined to the core. The temperature is inversely proportional to the distance from the nanorod (Online Methods), and thus sufficiently large particles undergo negligible surface heating. In contrast, mechanical energy is efficiently transmitted because of the cross-linked nature of the polymer. Three-dimensional simulations mapping particle temperature (**Fig. 1e** and **Supplementary Fig. 4**) confirmed that the OMA core collapses without significantly altering its surface temperature, thus minimizing thermal effects on cells.

To examine the dynamics of OMAs, we labeled the particles and recorded the fluorescence during pulsed NIR stimulation (**Fig. 1f**, **Supplementary Fig. 5** and **Supplementary Video 1**). Particle actuation was highly reversible and could be sustained for at least $10^6$ cycles. The collapse and swelling time constants were 1.3 ± 0.1 ms and 3.3 ± 0.2 ms (mean ± s.d.), respectively (**Supplementary Fig. 5e**,**f**). Therefore, optomechanical stimulation is 1–2 orders of magnitude faster than magnetic actuation[6–8].

To estimate the force applied by OMAs, we used DNA-based fluorescence tension probes[12] and found that particle collapse

[1]Department of Chemistry, Emory University, Atlanta, Georgia, USA. [2]Georgia Institute of Technology, George W. Woodruff School of Mechanical Engineering, Atlanta, Georgia, USA. [3]Georgia Institute of Technology, School of Materials Science and Engineering, Atlanta, Georgia, USA. [4]Department of Cell Biology, Emory University School of Medicine, Atlanta, Georgia, USA. [5]AFM Business Unit, Bruker Nano Surfaces, Santa Barbara, California, USA. [6]These authors contributed equally to this work. Correspondence should be addressed to K.S. (k.salaita@emory.edu).

RECEIVED 27 FEBRUARY; ACCEPTED 4 NOVEMBER; PUBLISHED ONLINE 14 DECEMBER 2015; DOI:10.1038/NMETH.3689

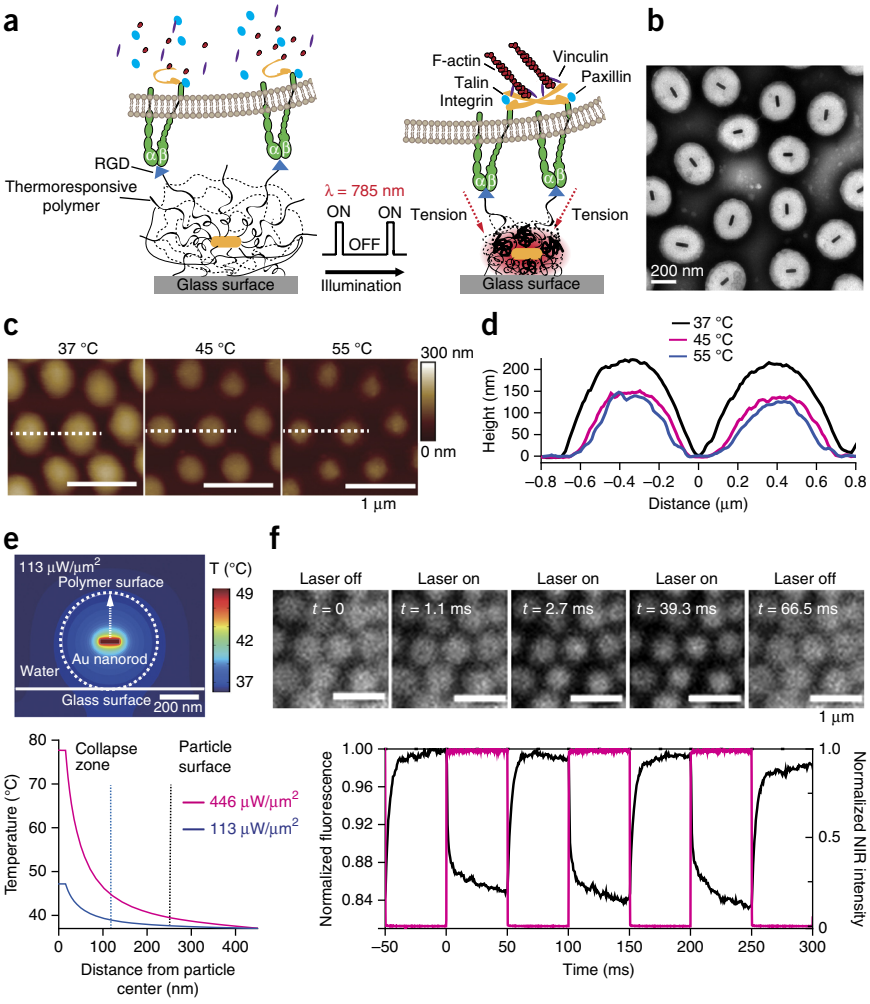


**Figure 1** | Schematic and characterization of optomechanical actuator (OMA) nanoparticles. (**a**) General design and proposed mechanism of OMA nanoparticles. (**b**) TEM image of OMA particles. (**c**) Atomic force microscopy (AFM) images of the OMA nanoparticles at different temperatures in deionized water. (**d**) Temperature-dependent height profile across two nanoparticles indicated by the dashed white line in **c**. Immobilized particles (at 37 °C) displayed a flattened morphology with a mean height and width of 220 and 700 nm, respectively. (**e**) Top, finite element simulation of the heat distribution in OMA nanoparticle irradiated with 785-nm NIR in water. Bottom, OMA particle temperature as a function of distance from the nanorod core irradiated at two different power densities (446 and 113 μW μm$^{-2}$). The power density (113 μW μm$^{-2}$) is tenfold greater than that used for cell stimulation to maintain the same peak power for the energy input calculation (Online Methods and **Supplementary Fig. 4**). (**f**) Top, OMA nanoparticles labeled with Alexa 488, captured by a sCMOS camera (Online Methods) at 1,800 fps while modulating the NIR laser source at 10 Hz (50% duty cycle). Data were collected in deionized water at 37 °C. Bottom, the average normalized fluorescence intensity (black curve) of OMA nanoparticles as the NIR laser (red curve) is modulated with a 10-Hz frequency and 50% duty cycle. The dynamics of fluorescence was used to estimate the time constant of particle collapse and relaxation. The ~15% decrease in fluorescence was primarily due to quenching by the gold nanorod (**Supplementary Fig. 5g,h**).

exerts a force per ligand of 13–50 pN (**Supplementary Fig. 6**). Given that integrin receptor forces within FAs are estimated within ~5–50 pN (refs. 12–14), OMAs are likely suited to triggering integrin activation. To test this, we transfected NIH/3T3 cells with a plasmid encoding GFP-paxillin, a surrogate marker for FAs[3,15]. We then cultured cells on a monolayer of OMA nanoparticles modified with cyclic Arg-Gly-Asp-d-Phe-Lys, c(RGDfK), with a density of 2,000 peptides μm$^{-2}$ for 12 h (**Supplementary Figs. 7–10**). We subsequently illuminated the particles under conditions that did not increase surface temperature (**Supplementary Fig. 11**) while recording GFP-paxillin dynamics (**Fig. 2a** and **Supplementary Video 2**). The total FA size grew from ~1 μm$^2$ to 5 μm$^2$ after stimulation for 17 min within region of interest (ROI) I, coinciding with the NIR illumination area (**Fig. 2a**,**b**). In contrast, the average FA size at ROI II, adjacent to the region of NIR stimulation, diminished by 50% during the same time period. FAs in ROI III, 20 μm away from the NIR source, did not change in size. Kymograph analysis and plots of total paxillin intensity over time within these ROIs confirmed this conclusion (**Fig. 2c**,**d**). Other markers of FAs, such as F-actin and vinculin, were also rapidly recruited upon identical NIR illumination (**Supplementary Fig. 12**), demonstrating FA assembly. F-actin polymerization precedes the recruitment of paxillin (GFP) and maturation of FA, in agreement with existing models (**Supplementary Fig. 13**). 3D structured illumination microscopy (3D-SIM) and total internal reflection fluorescence (TIRF) nanometry[16] showed that the actin network was mechanically displaced by ~100 nm following the collapse of particles (**Supplementary Figs. 3** and **14**). These results indicate that OMA collapse in the *x*, *y* and *z* directions mechanically strains integrin receptors and that this force is transmitted across the cell membrane, activating mechanosensitive proteins such as talin and vinculin, causing actin polymerization, and triggering FA maturation[3,8].

To rule out the effects of particle stiffness and ligand density in cell response, we treated GFP-paxillin–expressing cells with the Rho kinase (ROCK) inhibitor Y-27632 for 30 min (blocking myosin II contractility). ROCK inhibition attenuates stiffness sensing mechanisms and ligand density–driven FA maturation[3,17,18]. Within 5 min of particle actuation, cells rapidly protruded toward the source of the stimulus and increased GFP-paxillin density (**Fig. 2e** and **Supplementary Video 3**). Thus, OMA-driven cell response is independent of myosin contractility, and FA growth is primarily attributable to OMA-generated integrin forces (**Supplementary Note**).

To quantify cell response to the NIR frequency, we transiently transfected cells with LifeAct-mCherry, an F-actin probe. Cells showed a drastic enhancement in F-actin localization with OMA stimulation at frequencies of 10 and 100 Hz (**Fig. 2f** and **Supplementary Video 4**). In contrast, there was limited cell response at 1 Hz and 0 Hz (**Supplementary Figs. 15** and **16**). Therefore, for controlling FA formation, OMA nanoparticles require the application of cyclic mechanical stimulation rather than sustained force.

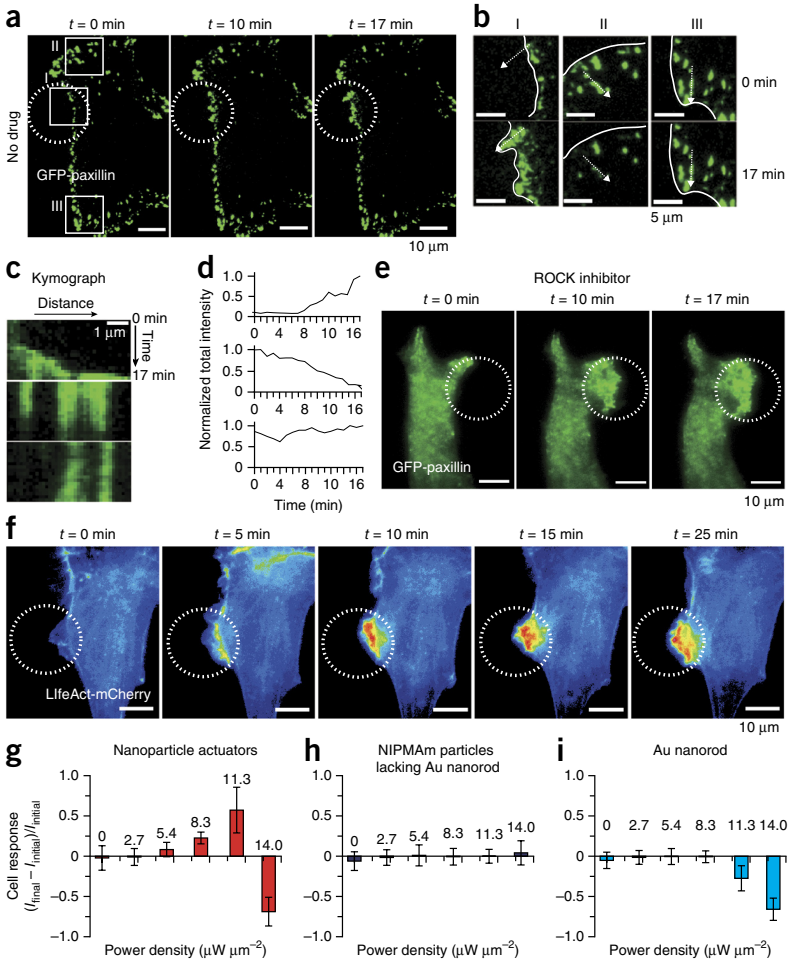


**Figure 2** | Optomechanical actuation of integrins leads to GFP-paxillin and LifeAct-mCherry recruitment. (**a**) Time-lapse TIRF images of NIH/3T3 cell transiently transfected with GFP-paxillin and cultured on OMA nanoparticles displaying the RGD peptide; $n \geq 5$ cells. White dashed circles represent region of NIR illumination (10 Hz, 10% duty cycle, power density = 11.3 μW/μm$^2$). (**b**) Zoom in the regions indicated with boxes in **a**. The white lines indicate the cell edge. (**c**) Kymograph (measured across dashed white arrows in **b**) and total paxillin intensity over time (**d**) within the regions of interest (ROI) I, II and III. (**e**) GFP-paxillin accumulation over time upon treatment with ROCK inhibitor. (**f**) Time-lapse fluorescence images of NIH/3T3 cells transiently transfected with LifeAct-mCherry upon NIR illumination (identical conditions to those used in **Fig. 2a**); $n \geq 20$ cells. The white dashed circles (in **e**,**f**) indicate the region of NIR illumination. (**g**–**i**) To quantify cell response to the NIR intensity and frequency, we transiently transfected cells with LifeAct-mCherry, an F-actin probe, and recorded actin intensity, $I = (I_{final} - I_{initial})/I_{final}$, where $I_{initial}$ is the total actin fluorescence in the ROI before stimulation, and $I_{final}$ is the total fluorescence in the same ROI following stimulation at $t$ = 20 min. Average cellular response for cells cultured on OMA nanoparticles (**g**), pNIPMAm particles lacking the gold rod core (**h**) and gold rods lacking the polymer shell (**i**), when the surface was excited by different NIR laser power intensities (10 Hz, 10% duty cycle). The error bar for each data point represents the s.d. of cell response from at least $n$ = 6 cells.

Illuminating particles at average powers >14.0 μW μm$^{-2}$ led to thermal heating and cell retraction (**Fig. 2g**; **Supplementary Figs. 11** and **17**). Also, particles that lacked the nanorod core (**Fig. 2h**), nanorods lacking the polymer shell (**Fig. 2i**) and nanorods coated with a thermally insensitive polymer (**Supplementary Fig. 18**) failed to generate a cell response regardless of the NIR intensity tested. These experiments further confirm that cell response is primarily driven by optical manipulation of integrin tension.

Given that FA formation ultimately controls cell protrusion and migration[19], we explored whether OMA stimulation could be used to guide cell movement. We stimulated FA formation in LifeAct-mCherry–transfected cells for 2 h (**Fig. 3a** and **Supplementary Video 5**). Initially (within 9 min), new protrusions formed in the illumination area. Subsequently (within 40 min), the cell migrated, presumably to maximize its overlap with the region of mechanical actuation. Regions of greatest F-actin intensity coincided with particle actuation. We then moved the illumination area such that at least one part of the cell maintained exposure to the mechanical stimulus. In this way, we mechanically guided the cell across the field of view. The average speed of cell migration was ~0.33 μm min$^{-1}$ (**Fig. 3b**,**c**). Although the approach is robust, there is cell-to-cell variability in response (**Supplementary Fig. 19**). Nonetheless, this experiment represents the first example of controlling cell migration by using active mechanical forces.

Recent single-molecule experiments showed that mechanical stimulation of the T cell receptor (TCR) activates T cells[20,21], and thus we next aimed to use OMA particles to optically control T cell activation. We modified OMA particles with the ovalbumin (OVA) antigenic peptide–major histocompatibility complex[20,21] (pMHC) and mechanically stimulated TCR in naive OT-I T lymphocytes (**Fig. 3d**). Within 1 min of NIR illumination, T cells displayed a calcium flux indicative of activation (**Fig. 3e**, **Supplementary Fig. 20** and **Supplementary Video 6**). OT-I cells optically stimulated on a pMHC monolayer on the glass coverslip showed no response (**Fig. 3f**,**g**). T cells rapidly respond to mechanical stimuli in contrast to cell adhesions, which typically require ~10 min for initial response.

In summary, we developed a new class of optomechanical actuator nanoparticles that allow for the spatial and temporal control of FA formation, cell migration and T cell activation. Control of cell migration using light has been achieved using optogentics[9,10], but unlike past examples, our approach precludes the need for genetic modification. Optomechanical stimulation represents a new avenue for controlling signaling activity in living cells ranging from neurons to platelets, and T cells. Moreover, the nontoxic nature of thermoresponsive polymers and gold nanoparticles suggests potential for *in vivo* applications.

## METHODS

Methods and any associated references are available in the online version of the paper.

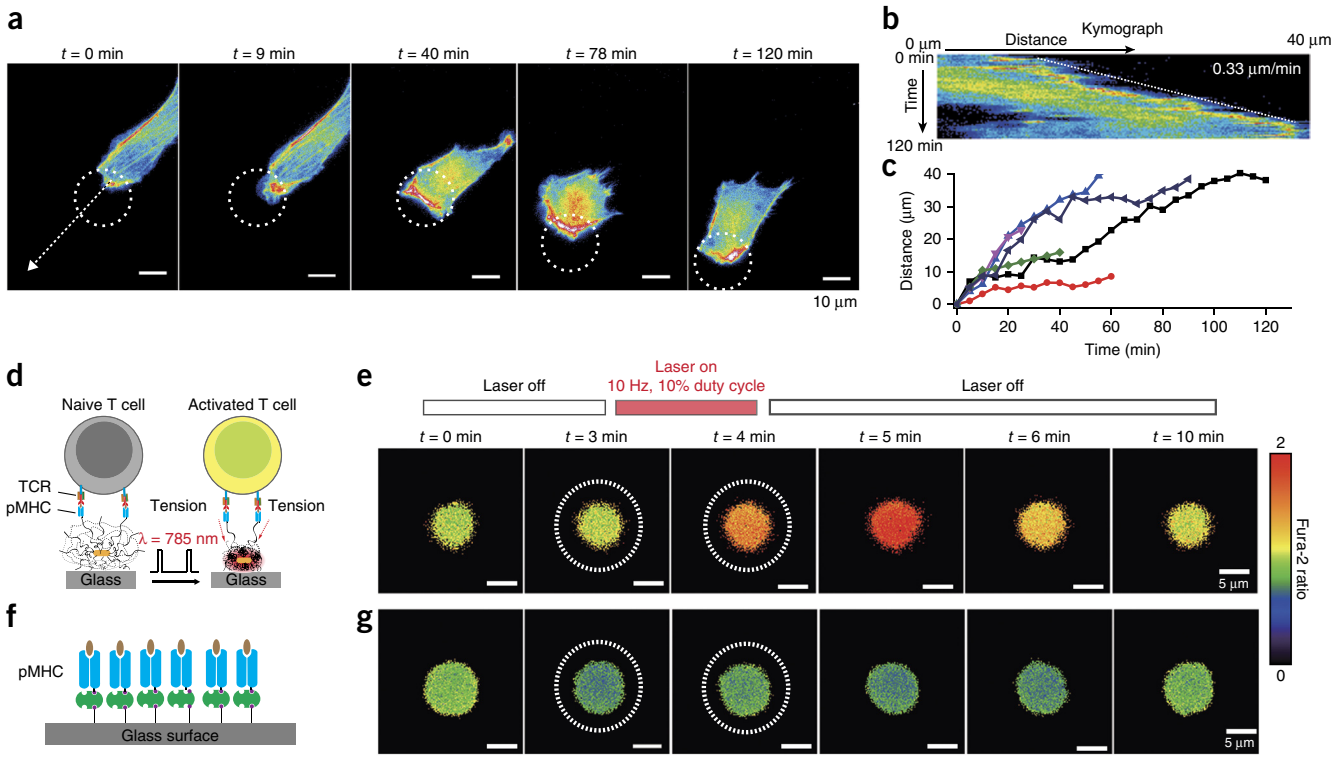


**Figure 3** | Optical control of cell migration and T cell activation by OMA nanoparticles. (**a**) Time-lapse images of NIH/3T3 cell migration in response to OMA stimulation. The white dashed circles represent the region of NIR illumination. (**b**) Kymograph analysis of cell migration measured in the direction of the white dashed arrow shown in **a**. Dashed line marks the edge of protrusion. (**c**) Cell migration distance as a function of time after OMA stimulation for $n = 6$ cells (**Supplementary Fig. 19**). Cell tracking was stopped when cells ceased to respond to NIR illumination or if cells displayed phototoxicity from fluorescence imaging. (**d**) Schematic showing OMA nanoparticles functionalized with the OVA pMHC and illuminated to mechanically stimulate T cell receptors in OT-I T lymphocytes. (**e**) Fluorescence images of the ratiometric intensity of the Fura-2 calcium indicator dye over time. Stimulation ($t = 3$ min, dotted white circles) was achieved using a 1-min NIR illumination duration. (**f**) Control experiments in which OT-I cells were stimulated on a pMHC monolayer on the glass coverslip. (**g**) Fura-2 fluorescence under control conditions in **f**. The white dashed circles (**e**,**g**) indicate the region of NIR illumination.

*Note: Any Supplementary Information and Source Data files are available in the online version of the paper.*


## ACKNOWLEDGMENTS

The authors are grateful for support from the US National Institutes of Health (R01-GM097399), the Alfred P. Sloan Research Fellowship, the Camille-Dreyfus Teacher-Scholar Award, the National Science Foundation (NSF) EAGER Award (1362113) and the NSF CAREER Award (1350829). This project was supported in part by the Emory University Integrated Cellular Imaging Microscopy Core. We thank M. Zhang for DLS data and S. Nie (Emory University and the Georgia Institute of Technology, Atlanta, Georgia, USA) for instrument access. We thank B. Evavold and L. Blanchfield (Emory University) for pMHC and T cells. We also thank C. Hill (Emory University) for access to the temperature-controlled visible-infrared spectrophotometer.


## AUTHOR CONTRIBUTIONS

K.S. and Z.L. devised the overall experimental strategy. Z.L. and Y.L. performed cell experiments and analyzed data. Z.L. synthesized and characterized the OMAs and developed the near-infrared laser illumination system for investigating the kinetics of OMAs and for single-cell-stimulation experiments. Y.L. synthesized molecular tension sensors. Y.C. and Y.L. synthesized the RGD-$N_3$ molecule. Z.L., Y.L., K.Y. and Y.Z. performed OMA modification. H.R.S. and A.H. performed the thermal simulations. A.L.M., Y.L. and Z.L. performed the 3D-SIM experiments and TIRF nanometry analysis. Z.H. performed temperature-controlled AFM. The manuscript was prepared by Z.L. and K.S. with input from all authors.

## COMPETING FINANCIAL INTERESTS

The authors declare no competing financial interests.




1. Vogel, V. & Sheetz, M. *Nat. Rev. Mol. Cell Biol.* **7**, 265–275 (2006).
2. Dufrêne, Y.F. *et al. Nat. Methods* **8**, 123–127 (2011).
3. Riveline, D. *et al. J. Cell Biol.* **153**, 1175–1186 (2001).
4. Charras, G.T. & Horton, M.A. *Biophys. J.* **82**, 2970–2981 (2002).
5. Wang, Y.X. *et al. Nature* **434**, 1040–1045 (2005).
6. Tseng, P., Judy, J.W. & Di Carlo, D. *Nat. Methods* **9**, 1113–1119 (2012).
7. Etoc, F. *et al. Nat. Nanotechnol.* **8**, 193–198 (2013).
8. Sniadecki, N.J. *et al. Proc. Natl. Acad. Sci. USA* **104**, 14553–14558 (2007).
9. Levskaya, A., Weiner, O.D., Lim, W.A. & Voigt, C.A. *Nature* **461**, 997–1001 (2009).
10. Wu, Y.I. *et al. Nature* **461**, 104–108 (2009).
11. Pastrana, E. *Nat. Methods* **8**, 24–25 (2011).
12. Zhang, Y., Ge, C., Zhu, C. & Salaita, K. *Nat. Commun.* **5**, 5167 (2014).
13. Salaita, K., Galior, K., Liu, Y., Yehl, K. & Vivek, S. *Nano Lett.* doi:10.1021/acs.nanolett.5b03888 (24 November 2015).
14. Jurchenko, C., Chang, Y., Narui, Y., Zhang, Y. & Salaita, K.S. *Biophys. J.* **106**, 1436–1446 (2014).
15. Oakes, P.W., Beckham, Y., Stricker, J. & Gardel, M.L. *J. Cell Biol.* **196**, 363–374 (2012).
16. Stabley, D.R., Oh, T., Simon, S.M., Mattheyses, A.L. & Salaita, K. *Nat. Commun.* **6**, 8307 (2015).
17. Coyer, S.R. *et al. J. Cell Sci.* **125**, 5110–5123 (2012).
18. Mih, J.D., Marinkovic, A., Liu, F., Sharif, A.S. & Tschumperlin, D.J. *J. Cell Sci.* **125**, 5974–5983 (2012).
19. Iskratsch, T., Wolfenson, H. & Sheetz, M.P. *Nat. Rev. Mol. Cell Biol.* **15**, 825–833 (2014).
20. Kim, S.T. *et al. J. Biol. Chem.* **284**, 31028–31037 (2009).
21. Liu, B.Y., Chen, W., Evavold, B.D. & Zhu, C. *Cell* **157**, 357–368 (2014).

## ONLINE METHODS

**Preparation of OMA nanoparticles.** *Gold nanorod preparation.* To generate OMA nanoparticles, we first synthesized the gold nanorod (NR) inorganic core using an improved seeded growth synthesis procedure, recently published by Murray and colleagues[22]. The synthesis of AuNRs employed a binary surfactant mixture composed of hexadecyltrimethylammonium bromide (CTAB) and sodium oleate (NaOL) to grow Au seed crystals into NRs. Briefly, the seed solution was prepared as follows: 5 mL of 0.5 mM $HAuCl_4$ was mixed with 5 mL of 0.2 M CTAB solution in a 20 mL scintillation vial. 0.6 mL of fresh 0.01 M $NaBH_4$ was diluted to 1 mL with water and was then injected into the Au(III)-CTAB solution under vigorous stirring (1,200 r.p.m.). The color of the solution changed from yellow to brownish yellow and the stirring was stopped after 2 min. The seed solution was aged at room temperature for 30 min before use.

We adapted the general guidelines presented by Murray *et al.*[22] to control the dimensions of the NR such that the NIR plasmon peak was approximately 800 nm. In our protocol, we prepared a growth solution comprised of 3.6 g of CTAB and 0.4936 g of NaOL dissolved in 100 mL of warm water (~50 °C) in a 250 ml Erlenmeyer flask. The solution was allowed to cool down to 30 °C, and then 8.5 mL of 4 mM $AgNO_3$ solution was added. The mixture was kept undisturbed at 30 °C for 15 min, after which 100 mL of 1 mM $HAuCl_4$ solution was added. The solution became colorless after 90 min of stirring (700 r.p.m.), and then 0.6 ml of HCl (37 wt. % in water, 12.1 M) was introduced to adjust the pH and acidify the solution. After 15 min of slow stirring at 400 r.p.m., 0.6 mL of 0.064 M ascorbic acid was added and the solution was vigorously stirred for 30 s. Finally, 80 µL of seed solution was injected into the growth solution. The resultant mixture was stirred for 30 s and left undisturbed at 30 °C for 12 h to complete NR growth. The products were isolated by centrifugation at 5,000 r.p.m. for 60 min followed by removal of the supernatant and washed with DI water. The final solution was concentrated to 90 ml and characterized using UV-vis-NIR and TEM.

*Polymerization and encapsulation of AuNRs with pNIPMAm.* The procedure for polymerization and encapsulation of the AuNRs with pNIPMAm[23] was adapted from methods noted by Contreras-Caceres *et al.*[24] and F. Tang *et al.*[25] employing Au and Ag spherical nanoparticles, respectively. First, the CTAB and NaOL surfactants coating the AuNRs were replaced with a thiolated and vinyl terminal (C = C) ligand by adding 20 mg of *N,N′*-bis(acryloyl)cystamine to a 90 ml AuNR solution along with 10 ml ethanol while vigorously stirring at 700 r.p.m. for 12 h. Subsequently, the AuNR solution was purified by centrifugation at 5,000 r.p.m. for 60 min, removing the supernatant, and then redispersing in 15 mL of deionized (DI) water. This solution could be stored at 4 °C for several months without adversely affecting quality of OMAs.

The polymerization of pNIPMAm on the Au nanorods surface was carried out as follows: 0.1 g of *N*-isopropylmethacrylamide, 0.01 g of the cross-linking agent *N,N′*-methylenebisacrylamide were dissolved in 15 ml Milli-Q water in a three-neck flask. The mixture was heated to 70 °C under continuous stirring and purged with continuous $N_2$ flow. Subsequently, 1 ml of the AuNR solution modified with the thiolated vinyl group (described above) was added to the three-neck flask. After 1 min, pNIPMAm polymerization was initiated with the addition of 80 µl (0.1 M) of the free radical initiator 2,2′azobis(2-methylpropionamidine) dihydrochloride (AAPH) and the polymerization was allowed to proceed for 2 h at 70 °C. In some cases, we aimed to decorate the OMA particles with the alkyne functional group. This was achieved by adding 30 µl of propargyl methacrylate monomer dissolved in 1 mL ethanol at the 100 min time point of reaction and allowing the free-radical polymerization to proceed for the full 2 h. Please note that vigorous stirring (1,200 r.p.m.) was used in every step in the OMA particle synthesis, and no additional detergent was used in the synthetic protocol. After the reaction was complete, the sample was allowed to gradually cool to room temperature while stirring. To remove gold-free nanoparticles, the dispersion was diluted with water and centrifuged, then the supernatant was removed and the resulting pellet was redispersed in water. The procedure was repeated at least three times, yielding OMAs with ~95% purity based on TEM analysis.

The synthesis of the control pNIPMAm particles with 50% cross-linking density used 40 mg of *N*-isopropylmethacrylamide and 40 mg of the cross-linking agent *N,N′*-methylenebisacrylamide; however, all other steps were identical to the protocol described above for the 10% cross-linking density pNIPMAm-coated particles. The synthesis of the control pNIPMAm particles lacking the inorganic Au NR core was identical to the protocol described above, with a single exception in that the 1 mL AuNR solution was not added.

**Characterization of OMAs.** Temperature controlled dynamic light scattering (DLS) was performed on a Zetasizer Nano ZS90 (Malvern Instruments, Malvern, UK). Negative staining transmission electron microscopy (TEM) was carried out on a Hitachi H-7500 transmission electron microscope at an accelerating voltage of 75 kV. AFM measurements were performed on a "FastScan Bio" AFM (Bruker, USA) in a closed liquid cell with the ability to control the temperature of the solution from room temperature to 55 °C. Silicon AFM tips (Bruker) with a tip radius of curvature = 12 nm were used to image the sample in PeakForce tapping mode.

**Determination of dynamics of OMA nanoparticles.** To determine the collapse and relaxation dynamics of OMA nanoparticles in response to light, we functionalized the particles with a fluorescent dye and used pulsed NIR excitation coupled with fluorescence imaging to monitor particle dynamics. Note that Alexa 488 was selected to record particle dynamics because of its known temperature independence, which was verified in **Supplementary Figure 5g,h**. Therefore, changes in fluorescence quantum yield (intensity) could be ascribed to OMA particle collapse rather than to local heating. The OMA nanoparticles were immobilized onto azide modified coverslips (as described in the surface preparation section). However, rather than modifying the remaining alkyne functional groups with the cRGDfK peptide, the OMA nanoparticles were conjugated with an azide-modified fluorescent dye. Briefly, a 50 µL solution containing 2.5 µL of 2 nM Alexa Fluor 488-cRGDfK-azide (note: the synthesis of this molecule was adapted from Liu *et al.*[26]). 2.5 µL of 10 mM ascorbic acid, 5 µL of 10 mM Cu(II)-TBTA (55% DMSO), and 40 µL of 55% (v/v) DMSO was placed between two OMA-modified coverslips. The sandwiched coverslips were sealed in a secondary petri dish, and the reaction was allowed to proceed for 12 h at room temperature.

The coverslips were then rinsed with ethanol and dried under a stream of nitrogen. The samples with Alexa 488–OMA particles were then simultaneously imaged using epifluorescence microscopy while chopping the NIR laser source at 10 Hz (50% duty cycle). A standard FITC cube was used for fluorescence imaging. In addition, two filters (product number: 87-745,47-291, Edmund optics, USA) were included in the optical path to block the NIR illumination. The fluorescence images were captured by a sCMOS camera (Zyla 4.2 sCMOS, Andor Technologies Ltd., UK) at 1800 fps.

**Determination of cRGDfK peptide density on OMA nanoparticles.** The value of the extinction coefficient for the cRGDfK peptide was too small for absorption spectrometry to quantify the peptide loading density. Instead, to estimate the peptide density, azide dye was coupled to the alkyne terminal group of the OMA nanoparticles using click chemistry. Based on the assumption that the dye and the cRGDfK peptide have similar coupling efficiencies, we quantified the dye loading density to approximate the peptide loading density.

*Quantitative fluorescence calibration curve using supported lipid bilayers.* In order to quantify the dye loading density, a quantitative fluorescence supported lipid bilayer calibration curve was constructed to relate fluorescence to dye density[27]. To establish the linear relationship between the observed fluorescence intensity and the fluorophore density, we prepared lipid bilayers with predefined concentrations of fluorescent lipid molecules. Non-fluorescent DOPC supported lipid membranes were doped with DPPE-fluoresce in lipids with ratios ranging from 0 to 1 mol% and then imaged under the same conditions used in live cell imaging (**Supplementary Fig. 9a**,**b**). The number of fluorophore molecules per unit area was directly calculated from the footprint of a DOPC lipid, which was reported at 0.72 $nm^2$ (ref. 27).

*Determination of the F factor.* The scaling factor *F* represents the ratio of FAM emission versus the DPPE-fluorescein emission and is defined as: $F = I_{bulk(FAM\text{-}azide)}/I_{bulk(DPE\text{-}fluorescein)}$, where $I_{bulk(FAM\text{-}azide)}$ and $I_{bulk(DPPE\text{-}fluorescein)}$ are the intensity of the ligand and lipid molecules in solution after being normalized for concentration, respectively. This value was measured on the fluorescence microscope by moving the focal plane (~200 μm) into the center of the sample (**Supplementary Fig. 9d**).

*Determination of FAM density on OMA nanoparticles surface.* To exclude fluorescence quenching by the Au NR core, 50 mM KCN was used to dissolve the gold NR core before covalent immobilization of the OMAs nanoparticles onto the glass substrate. After gold dissolution, OMA nanoparticles were washed 5 times with DI water by centrifugation (8,000 r.p.m., 10 min) to wash away the KCN. Subsequently, OMA nanoparticles without the AuNR core were covalently immobilized onto the azide functionalized glass substrates using the click reaction. In order to exclude fluorescence self-quenching, the FAM-azide concentration was ten times lower than the cRGDfK peptide concentration when functionalizing OMA particles. Briefly, a 50 μL solution containing 2.5 μL of 30 mM FAM-azide, 2.5 μL of 10 mM ascorbic acid, 5 μL of 10 mM Cu(II)-TBTA (55% DMSO, 45% $H_2O$), and 40 μL of 55% by volume DMSO were added to an OMA(Au NR free)-functionalized coverslip and sandwiched with a second OMA(Au NR free)-functionalized glass coverslip. This reaction was allowed to proceed at 50 °C for 3 h before rinsing with ethanol and drying with nitrogen. The surface was imaged under the same conditions used in live cell imaging. Using the calibration curve, *F* factor and fluorescence intensity from FAM labeled OMA (Au NR free)-functionalized coverslips (**Supplementary Fig. 9d**), FAM density was estimated to be ~2,000 molecules $\mu m^{-2}$. Note, because the FAM-azide reaction concentration is ten times lower than the cRGDfK peptide concentration used for cell experiments, the absolute RGDfK peptide density should be much higher than 2,000 molecules $\mu m^{-2}$, and this value represents the lower bound estimate.

**Estimation of OMA nanoparticle collapse-driven forces using molecular tension sensor.** To estimate the force applied during OMA nanoparticle collapse, we immobilized OMA nanoparticles onto a surface functionalized with DNA-based molecular tension probes that were recently developed in our lab[12,26,28]. The DNA tension sensor consists of three components: 1) a lower ssDNA strand modified with a molecular quencher (BHQ1) at the 3′ end, 2) an upper ssDNA strand modified with a Cy3B dye as fluorescence reporter at the 5′ end, 3) and a bridging hairpin duplex flanked by two complementary ssDNA arms that brings the BHQ1 and Cy3B into close proximity. Due to the high quenching efficiency (>95%) between BHQ1 and Cy3B dye, minimal fluorescence is detected when the hairpin is folded. However, when sufficient external forces are applied to the two ends of DNA, the hairpin structure becomes unfolded due to force, which effectively results in a physical separation of Cy3B dye away from BHQ1. This increased distance between dye and quencher is accompanied by a significant amount of fluorescence increase (~10- to 30-fold) due to de-quenching of the dye. Therefore, this method enables force measurements in real time. Here, we used a DNA hairpin that has been experimentally calibrated to have a $F_{1/2}$ of ~13 pN, which indicates that 50% of hairpins will unfold at a force = 13 pN.

To immobilize the DNA tension sensor to the coverslip, we adapted a previously published protocol for AuNP tension sensor[26]. Initially, 9 nm spherical AuNPs were randomly anchored to a lipoic acid modified glass coverslip. To efficiently attach the DNA tension sensors onto the AuNP coverslip with high coverage, we modified the sensor with a thiol group at the 5′ end of the lower ssDNA and directly incubated the sensor construct to the AuNP surface. Typically, 300 nM thiolated DNA hairpins in 1 M NaCl solution were incubated with the AuNP surface overnight. Note, all hairpin samples were pre-folded by applying an annealing cycle in PCR thermocycler. On the 3′ end of the upper ssDNA, we added an additional biotin group available to bind to streptavidin, which provides a link for the tension sensor to ultimately bind to the biotinylated OMA particles.

Upon NIR illumination of particles, we observed a reversible increase in fluorescence that coincided with NIR illumination. DNA unfolding could be repeated for hundreds of cycles until photobleaching of the force-reporting dye occurred. This suggested that the particle collapse exerts a force that is greater than 13 pN (force response threshold), but below the ~50 pN force required to shear DNA duplexes (**Supplementary Fig. 6**).

**Simulations.** Calculations of the OMA particle temperature and heat distribution were performed by finite element simulation (Comsol Multiphysics, Burlington MA). In all the simulations, the NIR laser power was held constant at 35 mW but with different radius of the laser spot (3, 5, 7, 10 μm, respectively). In these





doi:10.1038/nmeth.3689

simulations, we assume that during the transient laser heating period (10 msec), the temperature of the OMA particle reaches steady state conditions. Thus, we calculate the temperature distribution in the nanorod and polymer at steady state to determine the maximum temperatures that would be observed during the illumination cycle. We also assume that the nanorod is located exactly at the center of polymer and the laser illumination provides a constant and uniform heat generation that dissipates uniformly from the gold nanorod. The absorption cross section of Au NR was estimated at 20,000 $nm^2$ based on literature precedent[29]. The heat capacity and thermal conductivity of the polymer hydrogel is assumed to be equivalent to that of water[29]. The value of thermal conductivity of gold nanorod was set to 317 $W\,mK^{-1}$ (ref. 30). Note that the power density of 113 $\mu W\,\mu m^{-2}$ (35 mW, the radius of the laser spot was 10 µm, 100% duty cycle) is 10-fold greater than that used for cell stimulation because a 100% duty cycle (steady state illumination) is assumed for the energy input calculation.

**Surface preparation.** Glass coverslips (No. 2–25mm diameter, VWR) were sonicated in Nanopure water (18.2 mΩ) for 10 min and then etched in piranha for 10 min—please take caution, as piranha is extremely corrosive and may explode if exposed to organics. The glass coverslips were then washed twice in a beaker of Nanopure water (18.2 mΩ) and placed into three successive wash beakers containing ethanol and left in a final fourth beaker containing 1% 6-azidosulfonylhexyl-triethoxysilane (Gelest, Inc.) in ethanol for 6 h. The azide functionalized substrates were then immersed in the ethanol three times and subsequently rinsed with ethanol and dried under $N_2$. To covalently immobilize the OMAs nanoparticles (or pNIPMAm particles lacking the Au NR core) onto the azide functionalized glass substrates, a 50 µL solution containing 10 µL of 1 nM OMA nanoparticles,10 µL of 10 mM ascorbic acid, 10 µL of 10 mM Cu(II)-TBTA(55% DMSO), and 20 µL of DMSO were added onto one azide modified glass coverslip and then covered using a second azide functionalized glass coverslip. The sandwiched coverslips were sealed in a secondary petri dish, and the reaction was allowed to proceed for 12 h at room temperature. The coverslips were then rinsed with ethanol and dried under a stream of $N_2$. This procedure generated coverslips coated with a monolayer of covalently immobilized OMA particles. To further modify OMA particles with the cyclic Arg-Gly-Asp-d-Phe-Lys c(RGDfK) peptide, a 50 µL solution containing 2 µL of 318 mM RGD-$N_3$, 5 µL of 10 mM ascorbic acid, 5 µL of 10 mM Cu(II)-TBTA (55% DMSO), and 40 µL of 55% (by volume) DMSO was sandwiched between two OMA-functionalized substrates. This reaction was allowed to proceed at 50 °C for 3 h before rinsing with ethanol and drying with nitrogen.

To prepare Au NRs lacking the polymer shell, the CTAB and NaOL surfactants coating the AuNRs were exchanged with 1 mM alkyne terminated PEG thiol (Catalog number: PG2-AKTH-1k, 1000 g/mol, Nanocs, USA) in a 1 ml AuNR solution (described in *Gold nanorod preparation*). To allow for more complete ligand exchange, the solution was sonicated for 3 min and left at room temperature for 12 h. Subsequently, the AuNR solution was purified by centrifugation at 5,000 r.p.m. for 10 min, removing the supernatant, and then redispersing in 25 µl of deionized water. These Au NRs were immobilized onto azide-functionalized glass coverslips by placing a 70 µL solution containing 25 µl of Au NRs modified with the alkyne terminal group, 5 µL of 10 mM ascorbic acid, 5 µL of 10 mM Cu(II)-TBTA(55% DMSO), and 35 µL of DMSO between two coverslips. The sandwiched coverslips were sealed in a secondary petri dish, and the reaction was allowed to proceed for 12 h at room temperature. The coverslips were then rinsed with ethanol and dried under a stream of nitrogen. The coverslips were subsequently incubated with 500 µL of 100 $\mu g\ ml^{-1}$ human fibronectin (Sigma-Aldrich) for 1 h. Fibronectin enhanced cell binding to the bare AuNR surface to allow for control experiments. Coverslips were rinsed with sterile PBS before seeding cells and conducting experiments.

**Synthesis of RGDfK-$N_3$.** 500 µg of cRGDfK peptide (Peptides International, MW: 603.68) was reacted with 1.2 mg azide-NHS linker (Thermo Scientific. MW: 198.14) in 20 µL DMF. To this reaction mixture, 0.1 µL of neat triethylamine was added as an organic base and the reaction was allowed to proceed for 12 h at room temperature. The product was purified by reverse phase HPLC (flow rate 1 ml/min; solvent A: 99.5% DI water, 0.5% TFA; solvent B: 99.5% acetonitrile 0.5% TFA; initial condition was 10% B with a gradient of 1% per min). The final RGDfK-$N_3$ product was verified by MALDI-TOF.

**Cell culture and transfection.** NIH/3T3 fibroblast cells were cultured in Dulbecco's Modified Eagle's Medium (DMEM) supplemented with 10% Cosmic Calf Serum (Mediatech), HEPES (9.9 mM, Sigma), sodium pyruvate (1 mM, Sigma), L-glutamine (2.1 mM, Mediatech), penicillin G (100 IU $ml^{-1}$, Mediatech) and streptomycin (100 $\mu g\ ml^{-1}$, Mediatech) and were incubated at 37 °C with 5% $CO_2$. Cells were passaged at 60–80% confluency and plated at a density of 10% using standard cell culture procedures. All cell transfection was performed in a 24-well plate. All procedures are based on a standard protocol provided by Life Technologies (Carlsbad, CA). Briefly, $4 \times 10^4$ cells were plated in each well one day before transfection. During transfection, 0.5–1 g DNA was mixed with Lipofectamine LTX with Plus Reagent for each well and incubated for 24–48 h before imaging.

**Microscopy and optomechanics experiments.** Transfected NIH/3T3 cells were cultured on a monolayer of OMA nanoparticles modified with cyclic Arg-Gly-Asp-D-Phe-Lys c(RGDfK) with a density of 2,000 peptides per $\mu m^2$ for 12 h. Live cells were imaged in standard cell imaging buffer (Hank's balanced salt, pH 7.4, 10 mM HEPES without phenol red) at 37 °C. During imaging, physiological temperature was maintained with a warming apparatus consisting of a sample warmer and an objective warmer (Warner Instruments 641674D and 640375). The microscope was Nikon Eclipse Ti driven by the Elements software package. The microscope features an Evolve electron multiplying charge coupled device (EMCCD; Photometrics), an Intensilight epifluorescence source (Nikon), a CFI Apo 100× (numerical aperture (NA) 1.49) objective (Nikon) and a TIRF launcher with three laser lines: 488 nm (10 mW), 561 (40 mW), and 638 nm (20 mW). The experiments used the following Chroma filter cubes: TIRF 488, TRITC, FITC and reflection interference contrast microscopy (RICM). For optomechanics experiments, a near-infrared diode laser (Schäfter+Kirchhoff, Hamburg, Germany) was mounted using the standard dark-field condenser accessory available from

Nikon. The NIR laser wavelength was 785 nm ± 10 nm, while the laser output maximum power was 53 mW. The minimum size (diameter) of the focused spot was 6 µm. The laser modulation frequency was controlled by a frequency generator following the instructions provided by the manufacturer. Two additional NIR cutoff filters (product number: 87-745, 47-291, Edmund optics, USA) were included into the optical path to eliminate NIR blead through to the EMCCD. Using this setup, we simultaneously illuminated the sample with a pulsed NIR source (10 Hz, 10% duty cycle) while recording FAs dynamics for the cell.

**Calcium imaging.** To modify the OMA surface with peptide–major histocompatibility complex (pMHC), the amine functionalized OMA particles were incubated with NHS-biotin (Thermo Fisher) at 2 mg $ml^{-1}$ in DMSO (Sigma) overnight. Subsequently, the substrates were washed with EtOH and dried under a stream of nitrogen. This was then followed by incubation with streptavidin (1 µg $ml^{-1}$, 1 h and room temperature). After rinsing with PBS, the substrates were incubated with the biotinylated H-2K(b) monomers (80 µg $ml^{-1}$, 1 h, room temperature). After final rinsing with PBS, the substrates were assembled into the cell imaging chamber (Life Technologies), replaced with Hank's balanced salt imaging buffer (Sigma) and used immediately for cell experiments. Here, biotinylated H-2K(b) monomers were provided by the National Institutes of Health Tetramer Core Facility at Emory University. Monomers are comprised of the cognate chicken ovalbumin 257-264 epitope SIINFEKL (N4) peptide loaded in the alpha chain of mouse H-2K(b) that is complexed with beta-2-microglobulin (b2m) from mouse origin.

Freshly purified OT1 cells ($n = 1 \times 10^6$) were centrifuged to remove the RPMI media and re-suspended in 3 ml of Hank's imaging buffer. 10 µL of 1 mM of Fura-2/Am in DMSO was added into the cell suspension. The solution was kept at 37 °C for 30 min. Afterwards, cells were pelleted by centrifugation at 1,200 r.p.m. for 4 min and re-suspended in 3 ml of imaging buffer for an additional 15 min. This step is to ensure full de-esterification of the Fura-2/Am. Then, the cells were again pelleted and re-suspended in 1 ml of imaging buffer and prepared for seeding on the OMA surface. The cells were incubated for 20 min before stimulation.

For the calcium imaging, the microscope employed a Nikon CFI S Fluor 100x oil objective, a Chroma 340 excitation filter set (ET340x, T400lp and ET510/80m) and Chroma 380 excitation filter set (ET380x, T400lp and ET510/80m). During the experiment, the fluorescence images were acquired by using the 340 nm and 380 nm filter sets sequentially. Afterwards, ImageJ was used to generate a mask for both channels excited by 340 nm and 380 nm. Finally, the Fura-2 ratio (I340/I380) was calculated by using the image calculator function in ImageJ.

**Determination of F-actin displacement using TIRF-based nanometry.** The evanescent field intensity in TIRF exponentially decays with a predictable function[16,31],

$$I = I_0 e^{-z/d} \text{ and } d = \frac{\lambda}{4\pi\sqrt{n_1^2 \sin\theta^2 - n_2^2}}$$

where $I_0$ is the intensity at $z = 0$, $n_1$ and $n_2$ are the indices of refraction of the glass coverslip and the sample, respectively, $\lambda$ is the excitation wavelength, and $\theta$ is the angle of incidence. Therefore, one can infer the height changes of cellular structures, as long as the number of fluorophores remains fixed[31]. In our experiments, we assumed that $n_1$ (glass) = 1.515, $n_2$ (cell) = 1.37, $\lambda$ = 488 nm, $\theta$ = 70°–78°. Experimentally, we found that the TIRF intensity of F-actin increased by 70% ± 12% under steady-state NIR illumination (**Supplementary Fig. 14**). Using these parameters, and assuming an initial height of the F-actin at 220 nm, and fixed number of GFP emitters, we were able to estimate the change in height for the F-actin network. The height changes of the F-actin network are estimated to range between 95–115 nm in response to OMA particle collapse. Note that the $n_2$ is assumed to remain constant. However, the index of refraction for pNIPMAm is known to increase following collapse[29]. An increase in $n_2$ will reduce the value of $I$. Therefore, the calculated decrease in $z$ represents the minimum displacement.


22. Ye, X., Zheng, C., Chen, J., Gao, Y. & Murray, C.B. *Nano Lett.* **13**, 765–771 (2013).
23. Das, M., Sanson, N., Fava, D. & Kumacheva, E. *Langmuir* **23**, 196–201 (2007).
24. Contreras-Caceres, R. *et al. Adv. Mater.* **20**, 1666–1670 (2008).
25. Tang, F., Ma, N., Wang, X., He, F. & Li, L. *J. Mater. Chem.* **21**, 16943–16948 (2011).
26. Liu, Y., Yehl, K., Narui, Y. & Salaita, K. *J. Am. Chem. Soc.* **135**, 5320–5323 (2013).
27. Galush, W.J., Nye, J.A. & Groves, J.T. *Biophys. J.* **95**, 2512–2519 (2008).
28. Stabley, D.R., Jurchenko, C., Marshall, S.S. & Salaita, K.S. *Nat. Methods* **9**, 64–67 (2012).
29. Rodríguez-Fernández, J., Fedoruk, M., Hrelescu, C., Lutich, A.A. & Feldmann, J. *Nanotechnology* **22**, 245708 (2011).
30. Ekici, O. *et al. J. Phys. D Appl. Phys.* **41**, 185501 (2008).
31. Saffarian, S. & Kirchhausen, T. *Biophys. J.* **94**, 2333–2342 (2008).






doi:10.1038/nmeth.3689